Journal of Aircraft
Vol. 46, No. 2, March–April 2009

Engineering Notes

ENGINEERING NOTES are short manuscripts describing new developments or important results of a preliminary nature. These Notes should not exceed 2500 words (where a figure or table counts as 200 words). Following informal review by the Editors, they may be published within a few months of the date of receipt. Style requirements are the same as for regular contributions (see inside back cover).

Smart Spring Control of Vibration on Helicopter Rotor Blades

Gregory Oxley,* Fred Nitzsche,† and Daniel Feszty‡
Carleton University, Ottawa, Ontario K1S 5B6, Canada

DOI: 10.2514/1.27914

Nomenclature

c_1, c_2	=	Smart Spring viscous damping coefficients associated with primary and secondary load paths
F	=	external (input) force applied to the Smart Spring
k	=	effective dynamic stiffness of the Smart Spring
k_1, k_2	=	Smart Spring constants associated with primary and secondary load paths
m	=	effective inertia of the Smart Spring
m_1, m_2	=	mass of external and internal sleeves in the Smart Spring
N	=	contact force applied by piezoelectric stack
T	=	Smart Spring period of actuation
t	=	time
x	=	displacement (output) yielded by the Smart Spring
y	=	displacement associated with the Smart Spring secondary load path
κ	=	dynamic stiffness complex coefficients
μ	=	dry friction coefficient
Ω	=	Smart Spring control frequency, $2\pi/T$
ω	=	Smart Spring frequency of excitation

Superscripts

$\dot{}$	=	time derivative
$*$	=	complex conjugate

I. Introduction

HELICOPTERS generate significant vibration and noise, which deteriorates their operational economics and performance. The main sources of vibration are the rotor hub reactions of the inertial and aerodynamic loads on the rotor blades. In a rotor composed of identical blades, the rotor hub cancels most of the vibratory loads except for the harmonic multiples of the number of blades.

Active control of aeroelastic response and helicopter blade vibration has been a matter of great interest in the helicopter industry and the scientific community in general. In particular, individual blade control (IBC) [1] has gained special attention with the development of actuators capable of performing satisfactorily in a rotating frame reaching a significant degree of maturity. In recent years, several actuation schemes have been proposed, most of them based on solid-state actuators [2]. It is still a challenge, however, to produce solid-state actuators that can provide satisfactory results for full-scale helicopters. The main limitation is generally recognized to be the lack of sufficient control actuation power when full-scale aerodynamic and inertial loads are present. The piezoelectric materials, from which most solid-state actuators are built, are characterized by large specific energy. However, this energy is not readily available at the frequencies requested by IBC. Recent results indicate that active composite fibers (ACF) made from piezoelectric material embedded in host composite matrices may produce enough strain near the structural resonance, reaching the threshold of applicability in full-scaled blades [3]. The IBC concept using piezoelectric stacked material in combination with a mechanic amplification device was used to activate a flap successfully flown in a full-scale rotor [4].

Smart materials are characterized by a limited stroke, although they are able to generate a considerably large force. To circumvent this problem, the use of "smart" springs to indirectly achieve control over the vibration problem encountered in helicopter rotors has been proposed [5]. The Smart Spring is best suited for use in actively altering the boundary conditions of a beam structure and, as such, it should be incorporated at the root of the blade acting as a mechanical filter to attenuate the vibrations induced by the unsteady aerodynamic loads passing to the rotor hub. Although it can be used in any rotor configuration (hinged or hingeless) alone, it is better to use it in an IBC system cooperating with another flow-control device such as a servo flap or an ACF-embedded blade [6]. European and U.S. patents were granted to the National Research Council of Canada (NRCC) for the Smart Spring [7], and experiments in both still air and a wind tunnel for a nonrotating, full-scale blade were conducted at NRCC with a prototype actuator to verify its performance [8]. An independent investigation demonstrated that small changes in the nominal stiffness of the blade root are sufficient to attenuate all vibration loads up to a 90% efficiency [9]. This is not an unexpected result because modifying the boundary conditions has, in general, a significant effect on the vibration characteristics of a mechanical system.

The present paper explores the Smart Spring as a means of attenuating helicopter airframe vibration. This is achieved by modeling the Smart Spring as a replacement for the conventional rotor pitch link connecting the swash plate and blade pitch horn in SMARTROTOR, an advanced aeroelastic/aeroacoustic simulation tool for actively controlled rotors developed in a partnership involving Carleton University, the National Technical University of Athens in Greece, and the Massachusetts Institute of Technology in the United States [10]. In the present application, the structural model is based on the classical linear three-dimensional Euler beam theory attributable to Houbolt and Brooks [11], enhanced to include rigid-body modes due to the blade articulation. The aerodynamic model employs a discrete vortex-particle description of the flow that takes into consideration the free-wake characteristics, coupled with a panel method representation of the rotor blades [12]. In SMARTROTOR,

Presented as Paper 2270 at the 46th AIAA/ASME/ASCE/AHS/ASC Structures, Structural Dynamics and Materials Conference, Austin, Texas, 18–21 April 2005; received 21 September 2006; revision received 18 October 2008; accepted for publication 19 October 2008.

*Research Assistant, Department of Mechanical and Aerospace Engineering. Student Member AIAA.

†Professor, Department of Mechanical and Aerospace Engineering; fred_nitzsche@carleton.ca. Senior Member AIAA.

‡Assistant Professor, Department of Mechanical and Aerospace Engineering. Member AIAA.

the Farassat 1A formulation of the Ffowcs–Williams and Hawkings's equation generates the aeroacoustic results after the pressure distribution on the blades is obtained [13]. SMARTROTOR was validated against the experimental results produced by the European HELINOISE program in a previous publication [14].

II. The Smart Spring Principle

The Smart Spring principle is summarized in Fig. 1, in which two springs, k_1 and k_2, are associated with two load paths (primary and secondary, respectively). External and internal sleeves of masses m_1 and m_2, respectively, compose the assembly on the right-hand side of the figure. The latter sleeves can slide with respect to each other, preventing the two springs from being connected. An external force, $F(t)$, is applied to the external sleeve, which is attached to the spring designated by k_1. A stack of piezoelectric actuators is inserted into the internal sleeve, which is attached to the spring designated by k_2. When the actuators are off, the two sleeves can move freely and the resulting displacement is $x_{\max} = F/k_1$. When the actuators are turned on, the stack compresses the internal sleeve by a normal force, N. Only when the resultant friction force, μN, applied by the internal sleeve on the external sleeve is sufficiently large and the two sleeves are forced together is an arrangement of two springs in parallel obtained. The resulting displacement decreases to its minimum, $x_{\min} = F/(k_1 + k_2)$. Therefore, the stiffness of the system rises from its original value, k_1, to the final value, $k_1 + k_2$. In fact, the spring designated by k_2 is forced into motion by the resultant friction force applied by the internal on the external sleeve, which can be controlled by the external electrical stimulus. The displacement of the system under the external force varies between the two extremes, $x_{\min}$ and $x_{\max}$. In general, depending on the dimensions and manufacturing tolerances of the system, maximum displacement may not even be achievable because the maximum stroke supplied by the stack of piezoelectric elements might be insufficient to guarantee that the two sleeves move freely in the actuators-off condition.

When motion is involved during the actuation cycle defined by the electric stimulus, the friction coefficient varies between its highest (static) and its lowest dynamic limits. The actual variation process may be complicated, and the problem is more suitable to be treated experimentally rather than analytically. As an approximation, one can assume a process in which dry friction or "structural" damping is present. In fact, one may not expect that a perfect contact between the two sleeves will ever occur; therefore, some slippage always exists. This slippage, however, is beneficial to the robustness of the system because otherwise an on–off type of control would be present, implying that during the transients many blade structural modes could be excited.

The Smart Spring is a single-input, single-output system (SISO) in which the total displacement x (output) "seen" by the external harmonic force F (input) at any time is governed by Eq. (1),

$$m\ddot{x} + k(t)x = Fe^{i\omega t} \tag{1}$$

assuming that the inertia of the SISO system is represented by $m = m_1 + m_2$ and the magnitude of the resulting dynamic stiffness parameter varies between the two static limits, $k_1 \leq |k(t)| \leq k_1 + k_2$, according to a control law that may or may not be harmonic.

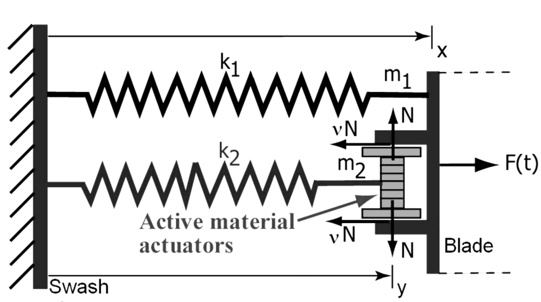

Fig. 1 Smart Spring principle.

It is worthwhile to stress that the variation on the dynamic stiffness parameter is directly proportional to the electrical stimulus, which is externally applied to the piezoelectric stack. In the simpler case, the control law is harmonic and, as such, it can be expanded into a complex Fourier series:

$$k(t) = \sum_{r=-\infty}^{r=\infty} \kappa_r e^{ir\Omega t} \qquad \kappa_r = 1/T \int_0^T k(t) e^{-ir\Omega t}\,\mathrm{d}t \qquad (r = 1, 2, \ldots, \infty) \tag{2}$$

As discussed earlier, the coefficients in Eq. (2) are best obtained from experimental characterization. The analytical solution of this dynamic problem is well known because it represents a linear differential equation with periodic coefficients, which is solved by the Floquet method [15]. Another solution to the same problem was presented in a previous work using the harmonic balance method and Hill's infinite determinants [16]. The latter solution is particularly interesting to pursue here because it helps to understand the proposed form of control. It is assumed that the solution is harmonic on the exciting frequency:

$$x(t) = \sum_{r=-\infty}^{\infty} x_r e^{ir\omega t} \tag{3}$$

The coefficients associated with the negative harmonics are simply the complex conjugates of their positive harmonic counterparts ($x_{-r} = x_r^*$). For the sake of this demonstration, the control law will be composed by only the first harmonic. If the time-averaged value of the dynamic stiffness coefficient is κ_0, one has $k(t) = \kappa_1^* e^{-i\Omega t} + \kappa_0 + \kappa_1 e^{i\Omega t}$ because $\kappa_{-1} = \kappa_1^*$. Substituting the latter expression for $k(t)$ into Eq. (1), using Eq. (3), and setting the control frequency equal to the exciting frequency, $\omega = \Omega$,

$$\sum_{r=-\infty}^{\infty} [(-mr^2\omega^2 + \kappa_0)e^{ir\omega t} + \kappa_1^* e^{i(r-1)\omega t} + \kappa_1 e^{i(r+1)\omega t}]x_r = Fe^{i\omega t} \tag{4}$$

(This is actually the case for most applications involving helicopter IBC.)

A transformation in the dummy indices of the summation is performed next. In Eq. (4), the two terms involving frequency shifts are rewritten as

$$x(t) = \sum_{r=-\infty}^{\infty} x_r e^{i(r\mp 1)\omega t} = \sum_{r\pm 1=-\infty}^{\infty} x_{r\pm 1} e^{ir\omega t} = \sum_{r=-\infty}^{\infty} x_{r\pm 1} e^{ir\omega t} \tag{5}$$

Replacing the latter series into Eq. (4), the following is obtained:

$$\sum_{r=-\infty}^{\infty} [(-mr^2\omega^2 + \kappa_0)x_r + \kappa_1^* x_{r+1} + \kappa_1 x_{r-1}]e^{ir\omega t} = Fe^{-i\omega t} + Fe^{i\omega t} \tag{6}$$

In Eq. (6), the harmonic exciting force was expanded to include its mirror image, negative harmonic, to keep the series real valued ($F_{-1} = F_1 = F$). Applying harmonic balance, the following set of tridiagonal equations on the coefficients of the frequency response is obtained:

$$
\begin{bmatrix}
\ddots & \kappa_1^* & & & & & \\
\kappa_1 & -4m\omega^2+\kappa_0 & \kappa_1^* & & & & \\
 & \kappa_1 & -m\omega^2+\kappa_0 & \kappa_1^* & & & \\
 & & \kappa_1 & \kappa_0 & \kappa_1^* & & \\
 & & & \kappa_1 & -m\omega^2+\kappa_0 & \kappa_1^* & \\
 & & & & \kappa_1 & -4m\omega^2+\kappa_0 & \kappa_1^* \\
 & & & & & \kappa_1 & \ddots
\end{bmatrix}
\times \begin{Bmatrix} \vdots \\ x_{-2} \\ x_{-1} \\ x_0 \\ x_1 \\ x_2 \\ \vdots \end{Bmatrix} = \begin{Bmatrix} \vdots \\ 0 \\ F \\ 0 \\ F \\ 0 \\ \vdots \end{Bmatrix} \tag{7}
$$

An approximate solution for the lower harmonics of $x(t)$ is achieved by successively increasing the number of the harmonics retained. The numerical convergence is very fast, even if F is composed of a large number of harmonics. This is due to the narrow band nature of the system of equations. The band of the system is twice plus one the number of harmonics present in the control law (a control law with two harmonics would produce a system of band five). However, if the control law itself has fast convergence properties, that is, the relative importance of its higher harmonics is increasingly less (a fair assumption in any real case), the numerical convergence of the solution will remain fast. The first approximation for the solution in the present case involves solving a 3×3 set of equations on the harmonic coefficients with indices of -1, 0, and 1, respectively:

$$
\begin{gathered}
x_{-1} = x_1^* \qquad x_0 = \frac{-(\kappa_1 + \kappa_1^*)}{(-m\omega^2 + \kappa_0)\kappa_0 - 2\kappa_1\kappa_1^*} F \\
x_1 = \frac{(-m\omega^2 + \kappa_0)\kappa_0 + \kappa_1^2 - \kappa_1\kappa_1^*}{(-m\omega^2 + \kappa_0)[(-m\omega^2 + \kappa_0)\kappa_0 - 2\kappa_1\kappa_1^*]} F
\end{gathered} \tag{8}
$$

A set of discrete complex frequency response functions between the input excitation F and the output displacement x is obtained. The introduction of the Smart Spring caused an *active redistribution* of the dynamic response spectrum, whose first approximation is given by Eq. (8). Therefore, helicopter IBC using the Smart Spring concept is achieved by the spectral redistribution of the unsteady aerodynamic loads. Because in the present demonstration no viscous damping was included, dissipation is solely due to hysteretic damping.

As one can infer from this discussion, the present concept fundamentally differs from other concepts devised to control aeroelastic response and to perform IBC [17]. In the presented concept, the energy supplied by the piezoelectric elements is used to do *indirect* rather than *direct* work against the external forces. This is a general principle that is expected to reduce the demand of power that is normally imposed on piezoelectric and other smart materials at frequencies at which they are not well suited for use. It is worthwhile to point out that this type of use of the smart material is more demanding on the *force* rather than *stroke* supplied by the material, which certainly favors the piezoelectric inherent characteristics.

III. Smart Spring Model and Control Algorithm

Figure 1 represents the physical model of a linear Smart Spring proposed to replace the helicopter pitch link (connecting the root blade to the swash plate) to actively reshape the spectrum of some of the transmitted higher-harmonic loads (i.e., the ones generated by the aerodynamic excitation of the torsion structural mode of the blade in this case, which is known to lie in the range of 3–5/rev for a typical helicopter blade and, therefore, would be critical in a four-blade rotor) from the blade to the swash plate. As also suggested by the diagram of the Smart Spring in Fig. 1, the equations that govern the motion are

$$
\begin{aligned}
m_1\ddot{x} + c_1\dot{x} + k_1 x &= F(t) \mp \mu(t)N(t) \\
m_2\ddot{y} + c_2\dot{y} + k_2 y &= \pm\mu(t)N(t)
\end{aligned} \tag{9}
$$

where viscous damping coefficients are now introduced in the primary and secondary load paths, respectively. The upper or lower signs of the dry friction terms are used if $\dot{x} > \dot{y}$ or $\dot{x} < \dot{y}$, respectively, and $\mu(t)$ is a function of the absolute relative velocity between the sleeves, $|\dot{x} - \dot{y}|$, and the contact materials properties. This model has been extensively studied, and its validity was checked against the hardware experimental results in another publication [18]. When the piezoelectric stack actuation force is off, $N(t) = 0$, Eq. (9) is decoupled and the external load is transmitted solely through the primary load path. When the actuation force is on, the external load is shared between the primary and secondary load paths.

In the present work, the Smart Spring has been implemented as a subloop of the main aeroelastic calculations in SMARTROTOR (Fig. 2). It provides the boundary condition for the pitch degree of freedom of the structural module. In the main aeroelastic loop of SMARTROTOR, the aerodynamic module calculates the blade loading, determines the rigid-body motion of the blade, and feeds these results back to the aerodynamic module. This is done iteratively until convergence is reached. When the Smart Spring is introduced as a subloop in the main aeroelastic loop, the pitch link loads are passed as an input to the Smart Spring in the form of the external load. The discrete version of Eq. (9) is solved at each time step for the output displacement using an implicit Newmark algorithm. The change in the pitch due to the output displacement of the Smart Spring is then fed back to the structural module.

The control strategy implemented in this study is on–off and based on the goal of maximum energy extraction from the system [19]. At each time step, the relative velocities of m_1 and m_2 are examined and it is determined whether a control action will promote the motion of m_1, thereby adding energy to the system, or whether it will hinder the motion of m_1, thereby extracting energy from the system. This is done by verifying the sign of the product $\dot{y}(\dot{x} - \dot{y})$. If it is positive (or zero), the control system maintains $N(t) = 0$. Otherwise, if negative,

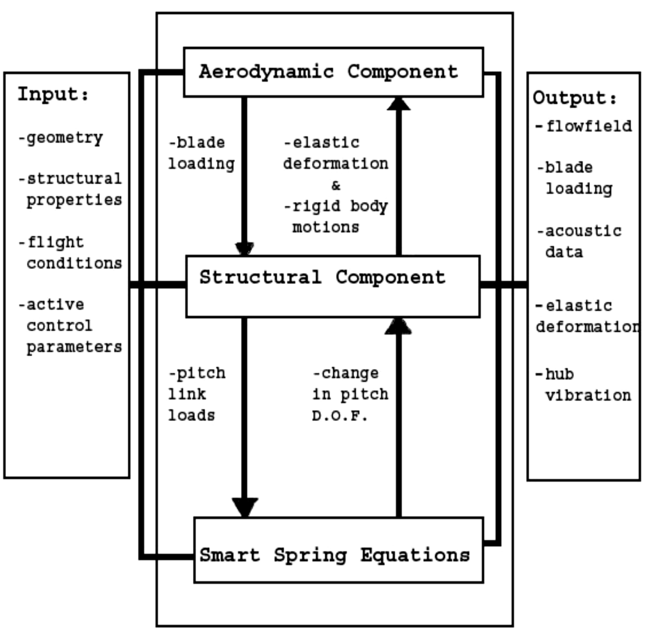

Fig. 2 SMARTROTOR code flowchart with Smart Spring device.

Table 1 Simulation Parameters

Blade geometry		Simulation parameters		Smart Spring constants	
No. blades	4	Time step	72/rev	m_1	0.500 kg
Blade planform	Rectangular	Rotor speed	109.22 rad/s	m_2	0.050 kg
Rotor radius	1.85 m	Advance ratio	0.25	c_1	1000 Ns/m
Chord length	0.121 m	Thrust trim	3875 N	c_2	200 Ns/m
Twist distribution	Linear (4 to −2 deg)	Moment trim	0 Nm	k_1	5.0×10^6 N/m
Airfoil type	NACA 23012	Revolutions	6	k_2	241 N/m
				$N_{\max}$	200 N

the control system sets $N(t) = N_{\max}$, the maximum possible value for the actuation force.

IV. Results and Analysis

The test case in which the Smart Spring will be demonstrated as a vibration attenuation device is based on the BO105 rotor. Table 1 summarizes the simulation parameters used in this analysis. The Smart Spring parameters were tuned to achieve the control strategy (maximum power extraction) at the frequency of 4/rev, which is considered critical for a four-blade rotor. Hence, in the primary load path, a linear spring of very high constant k_1 was set to guarantee the original stiffness of the pitch link and, thereof, the blade stability. The secondary load path was tuned to resonate at the 4/rev frequency.

Figure 3 depicts the axial load transmitted through the pitch link during one revolution of the rotor as predicted by SMARTROTOR (after six complete revolutions to achieve the steady-state condition). The value at 0/rev is the magnitude of the time-averaged force experienced by the pitch link. This value is the same for the controlled and uncontrolled situations, indicating that the Smart Spring, in fact, redistributes the vibration spectrum (arbitrarily truncated at 10/rev in the figure). The figure suggests that the Smart Spring acts as a filter for the higher harmonics of the axial load vibration spectrum, and it does not affect the harmonics associated with the rotor trim and cyclic control (0 and 1/rev, respectively) when its internal resonance is set at 4/rev. The small differences seen at 1 and 2/rev are due to numerical errors. The FFT analysis also indicates that harmonics higher than 2/rev were either attenuated or not considerably affected by the Smart Spring actuation. Significant reductions in the critical 4 and 8/rev (those multiples of the number of rotor blades) were verified.

V. Conclusions

Numerical simulation results indicated that the Smart Spring is a structural control device able to attenuate helicopter rotor higher-harmonic loads transmitted to the fuselage through the pitch link. The Smart Spring does not affect the rotor trim, collective and cyclic control commands if it is tuned to internally resonate at the rotor higher harmonic frequencies that are the objective of control. The force transmitted through the pitch link with the Smart Spring was verified to be 44% of the original value at 4/rev and 62% of the original value at 8/rev, which may be considered modest compared with other active vibration reduction approaches used in rotorcraft.

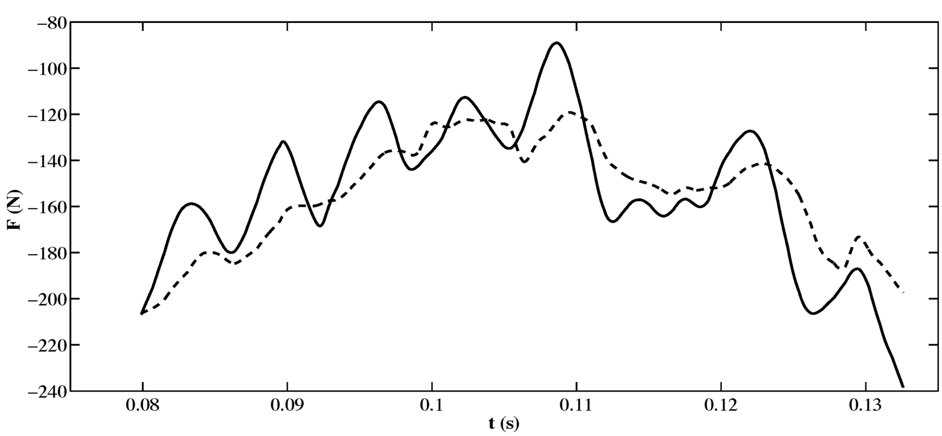

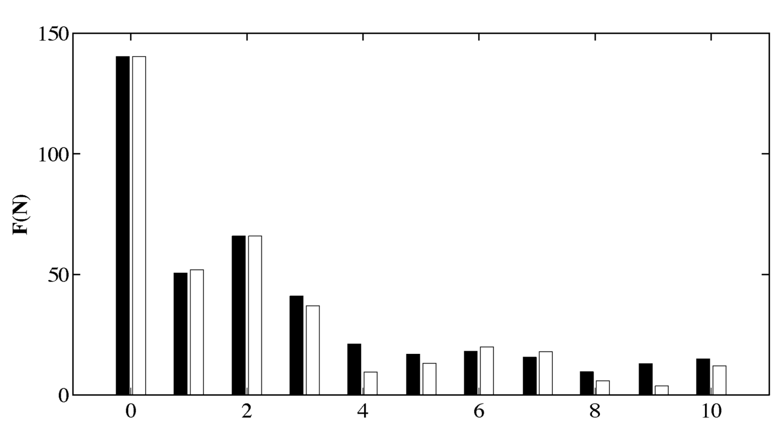

Fig. 3 Time history of the axial load transmitted through the pitch link with (dashed line) and without (solid line) the Smart Spring active control and corresponding FFT of the same data.

Acknowledgments

The authors would like to thank S. Voutsinas and V. Riziotis from the National Technical University of Athens for useful discussions and technical support for this project.

References

[1] Kretz, M., and Larche, M., "Future of Helicopter Rotor Control," *Vertica*, Vol. 4, pp. 13–22, 1980.

[2] Friedmann, P. P., and Millott, T. A., "Vibration Reduction in Rotorcraft Using Active Control: A Comparison of Various Approaches," *Journal of Guidance, Control, and Dynamics*, Vol. 18, No. 4, pp. 664–673. doi:10.2514/3.21445

[3] Wilbur, M. L., Yeager, W. T., and Sekula, M. K., "Further Examination of the Vibratory Loads Reduction Results From The NASA/Army/MIT Active Twist Rotor Test," *American Helicopter Society 58th Annual Forum*, Royal Aeronautical Society, Bristol, England, U.K., 2002, pp. 60.1–60.15.

[4] Jänker, P., Hermle, F., Lorkowski, T., Storm, S., and Wettemann, M., "Advanced Piezoelectric Servo Flap System for Rotor Active Control," National Aerospace Laboratory Paper AR-10, Sept. 2006.

[5] Nitzsche, F., Lammering, R., and Breitbach, E., "Can Smart Materials Modify the Blade Root Boundary Conditions to Attenuate Helicopter Vibration?," *Fourth International Conference on Adaptive Structures*, Technomic Publishing, 1994, pp. 139–150.

[6] Nitzsche, F., Feszty, D., Waechter, D., Bianchi, E., Voutsinas, S., Gennaraetti, M., Coppotelli, G., and Ghiringelli, G. L., "The SHARCS Project: Smart Hybrid Active Rotor Control System for Noise and Vibration Attenuation of Helicopter Rotor Blades," American Helicopter Society Paper 52, Sept. 2005.

[7] Nitzsche, F., Grewal, A., and Zimcik, D., "Structural Component Having Means for Actively Varying its Stiffness to Control Vibrations," U.S. Patent No. 5,973,440, October 1999.

[8] Yong, C., Zimick, D. G., Wickramasinghe, V., and Nitzsche, F., "Development of the Smart Spring for Active Vibration Control of Helicopter Blades," *Journal of Intelligent Material Systems and Structures*," Vol. 15, No. 1, pp. 37–47. doi:10.1177/1045389X04039655

[9] Anusonti-Inthra, P., and Ghandi, F., "Helicopter Vibration Reduction Through Cyclic Variations in Blade Root Stiffness," *Journal of Intelligent Material Systems and Structures*, Vol. 11, No. 2, pp. 153–166, 2000.

[10] Cesnik, C. E. S., Opoku, D. G., Nitzsche, F., and Cheng, T., "Active Twist Rotor Blade Modeling Using Particle-Wake Aerodynamics and Geometrically Exact Beam Structural Dynamics," *Journal of Fluids and Structures*, Vol. 19, pp. 651–668. doi:10.1016/j.jfluidstructs.2004.01.007

[11] Houbolt, J. C., and Brooks, G. W., "Differential Equations of Motion for Combined Flapwise Bending," *Chordwise Bending, and Torsion of Twisted Nonuniform Rotor Blades*, NACA Rept. 1346, 1958.

[12] Voutsinas, S. G., and Triantos, D. G., "High-Resolution Aerodynamic Analysis of Full Helicopter Configurations," American Helicopter Society Paper C11, Sept. 1999.

[13] Ffowcs-Williams, J. E., and Hawkings, D. L., "Sound Generation by Turbulence and Surfaces in Arbitrary Motion," *Philosophical Transactions of the Royal Society of London, Series A: Mathematical and Physical Sciences*, Vol. A264, pp. 321–342, 1969.

[14] Nitzsche, F., and Opoku, D. G., "Acoustic Validation of a New Code Using Particle Wake Aerodynamics and Geometrically Exact Beam Structural Dynamics," *The Aeronautical Journal*, Vol. 109, No. 1096, June 2005, pp. 257–267.

[15] Dugundji, J., and Wendell, J. H., "Some Analysis Methods for Rotating Systems with Periodic Coefficients," *AIAA Journal*, Vol. 21, pp. 890–897, 1983. doi:10.2514/3.8167

[16] Nitzsche, F., "Aeroelastic Analysis of a Helicopter Blade with Active Impedance Control at the Root," *Canadian Aeronautics and Space Journal*, Vol. 47, March 2001, pp. 7–16.

[17] Jacklin, S. A., Haber, A., deSimone, G., Norman, T. R., Kitaplioglu, C., and Shinoda, P., "Full-Scale Wind Tunnel Test of an Individual Blade Control System for a UH-60 Helicopter," *American Helicopter Society 58th Annual Forum*, American Helicopter Society, Alexandria, VA, June 2002.

[18] Harold, T., and Nitzsche, F., "The Smart Spring—An Indirect Active Low-Power Adaptive Structure Device for Vibration Attenuation," *High Performance Structures and Materials II*, edited by C. A. Brebbia and W. P. DeWilde, WIT Press, Southampton, England, U.K., 2004, pp. 297–306.

[19] Nitzsche, F., Harold, T., Wickramasinghe, V. K., Young, C., and Zimcik, D. G., "Development of a Maximum Energy Extraction Control for the Smart Spring," *Journal of Intelligent Material Systems and Structures*, Vol. 16, No. 11/12, pp. 1057–1066.